Crystal Structure of Alkaline Protease from Pseudomonas Aeruginosa IFO3455

AUTHOR(S):

Miyatake, Hideyuki; Hata, Yasuo; Fujii, Tomomi; Akutagawa, Tohru; Morihara, Kazuyuki; Katsube, Yukiteru

CITATION:

Miyatake, Hideyuki ...[et al]. Crystal Structure of Alkaline Protease from Pseudomonas Aeruginosa IFO3455. Bulletin of the Institute for Chemical Research, Kyoto University 1994, 72(3-4): 373-386

ISSUE DATE:

1994-11-30

URL:

http://hdl.handle.net/2433/77579

Bull. Inst. Chem. Res., Kyoto Univ., Vol. 72, No. 3-4, 1994

REVIEW

Crystal Structure of Alkaline Protease from *Pseudomonas Aeruginosa* IFO3455

Hideyuki MIYATAKE*, Yasuo HATA*, Tomomi FUJII*,
Tohru AKUTAGAWA*, Kazuyuki MORIHARA** and Yukiteru KATSUBE***

Received August 1, 1994

The three-dimensional structure of alkáline protease from *Pseudomonas aeruginosa* IFO3455, a zinc-requiring metalloprotease, has been determined by a multiple isomorphous replacement method of X-ray crystallography, and refined at 2.3 Å resolution to the R-factor of 0.198. The molecule has an elongated ellipsoidal shape with approximate dimensions of 90×42×35 Å. It consists of two distinct structural domains. The N-terminal domain is the proteolytic domain which contains the active site zinc atom in the inside of the large cleft. The overall structure of the domain is similar to that of astacin, a metalloprotease belonging to a superfamily different from that of the alkaline protease. The C-terminal domain has a two-layer β-sandwich structure consisting of 19 β-strands. In the central region of this domain is an unusual parallel β-helix structure in which successive β-strands are wound in a right-handed spiral through the short turns between the strands. Ca^{2+} ions bound internally within the turns formed by a repeated GGXGXD sequence motif may play an essential role in stabilizing this β-helix structure.

KEY WORDS: Alkaline protease/ X-ray analysis/ β-helix/ *Pseudomonas aeruginosa*/ Metalloprotease

1. INTRODUCTION

Alkaline protease from *Pseudomonas aeruginosa* IFO3455 is a zinc-requiring metalloendoprotease consisting of 470 amino acid residues[1,2] with one catalytic zinc atom.[3-4] Biochemical studies on the alkaline protease have revealed that the enzyme possesses a relatively wide specificity for substrates, and that the potential catalytic capability is optimized at pH 8 to 10,[5-6] which is unusual compared with other metalloendoproteases such as thermolysin, subtilisins, and neutral endopeptidases which are neutral in optimal pH. The pathologic aspects of the *P. aeruginosa* alkaline protease have been extensively investigated so far. The enzyme possesses potential anti-coagulant capacity to hydrolyze natural substrates of plasmin, such as fibrin and fibrinogen, with similar specific activities to plasmin.[7] From these properties of the enzyme, it is inferred that the *P. aeruginosa* alkaline protease may play a key role in infection of the bacteria to their host cells through inactivation of various physiological activators such as some complement components, immunoglobulins A and G, and many protease inhibitors.[8] Zinc-requring

* 宮武秀行, 畑 安雄, 藤井知実, 芥川 亨 : Division of Molecular Biology and Information I, Institute for Chemical Research, Kyoto University, Uji, Kyoto 611, Japan.
** 森原和之 : Institute for Applied Life Science, University of East Asia, Ichinomiya-Gakuen Cho 2-1, Shimonoseki, Yamaguch 751, Japan.
*** 勝部幸輝 : Institute for Protein Research, Osaka University, Suita, Osaka 565, Japan.

	176	177		180			183			186				
Serratia family														
alkaline protease[a]	**H**	**E**	I	G	**H**	T	L	**G**	L	S	**H**	P	G	D	Y
Serratia protease	**H**	**E**	I	G	**H**	A	L	**G**	L	S	**H**	P	G	D	Y
Erwina protease[b]	**H**	**E**	I	G	**H**	A	L	**G**	L	S	**H**	P	A	E	Y
Astatin family														
Astacin(cryfish)	**H**	**E**	L	M	**H**	A	I	**G**	F	Y	**H**	E	H	T	R
BMP1[c]	**H**	**E**	L	G	**H**	V	V	**G**	G	W	**H**	E	H	T	R
Meprin A	**H**	**E**	I	G	**H**	A	I	**G**	F	H	**H**	E	Q	S	R
Snake venom proteases														
Trimerelysin I	**H**	**E**	M	G	**H**	N	L	**G**	L	P	**H**	D	G	N	S
Atrolysin	**H**	**E**	L	G	**H**	N	L	**G**	M	E	**H**	D	G	K	D
Matrixin family														
Collagenase (human)	**H**	**E**	L	G	**H**	S	L	**G**	L	S	**H**	S	T	D	L
Stromelysin-1 (human)	**H**	**E**	L	G	**H**	S	L	**G**	L	F	**H**	S	A	N	T
Thermolysin family														
Thermolysin	**H**	**E**	L	T	**H**	A	V	T	D	T	T	A	G	L	I
Elastase (*P. aeruginosa*)	**H**	**E**	V	S	**H**	G	F	T	E	Q	A	S	G	L	I

Fig. 1. Sequence alignment near zinc-binding sites of zinc-endoproteases. The bold letters indicate conserved residues. The numbering of residues is based on that of *P. aeruginosa* alkaline protease. a) *Pseudomonas aeruginosa* alkaline protease; b) Erwinia chrysanthemi protease b; c) Human bone morphogenetic protein I.

metalloendoproteases could be classified into five families : *Serratia* protease family, snake venom protease family, matrixin family, astatin family, and thermolysin family. The enzymes of the first four families have the consensus sequence, HEXXHXXGXXH for zinc binding sites[9~10] (Fig. 1). The alkaline protease from *P. aeruginosa* belongs to the *Serratia* family because of the homology in amino acid sequence and physiological properties. A representative member of the *Serratia* family is *Serratia* protease from serratial bacteria, whose substrate preference and physiological effects on the foci resemble those of the *P. aeruginosa* alkaline protease. The alkaline protease shares about 55% homology in primary structure with *Serratia* protease whose tertiary structure has been analyzed by Dr. Hamada *et al.* of Shimane University in cooperation with us.[11] It is essential to analyze three-dimentional structures of enzymes which belong to the *Serratia* family to reveal structural features common to the family by structural comparison. In order to elucidate the structure-function relationship, molecular evolution and enzymatic characteristics of the family on structural viewpoints, we have analyzed the crystal structure of alkaline protease from *P. aeruginosa* IFO3455. Here we report the three-dimensional structure of the enzyme determined at 2.3 Å resolution by X-ray diffraction method.

2. MATERIALS AND METHODS

2.1 Crystallization

The lyophilized sample of alkaline protease from *P. aeruginosa* IFO3455, which was gifted from Nagase Biochemical Co. Ltd., was subjected to crystallization without further purification. Crystallization conditions were searched using a hanging drop vapor diffusion method, changing

protein concentration, nature and concentration of precipitant and buffer, pH and temperature. Crystals suitable for X-ray analysis were obtained by the following procedures using a 2% (w/v) protein solution and a reservoir solution of 6% (w/v) polyethylene glycol 6000. The protein solution was prepared by dissolving the lyophilized sample into a 1 mM NaN_3/5 mM $CaCl_2$ solution (pH 7.0). The reservoir solution was 50 mM acetate buffer (pH 5.6) containing 6% (w/v) polyethylene glycol #6000 (Nakarai Tesgue, Inc.) and 1 mM NaN_3. The droplets of protein solution used in the hanging drop method were prepared by mixing the protein solution and the reservoir solution in the volume ratio 1 : 1. In the first step of crystallization, small crystals were grown in a few days by vapor-equilibrating 5 μl of the protein droplet against 1ml of the reservior solution at 25°C. In the next step, a sitting drop vapor diffusion method was used under the same conditions as previous to make the crystals larger by a seeding technique. A larger droplet for seeding was prepared by putting one crystal into 60 μl of the same solution as

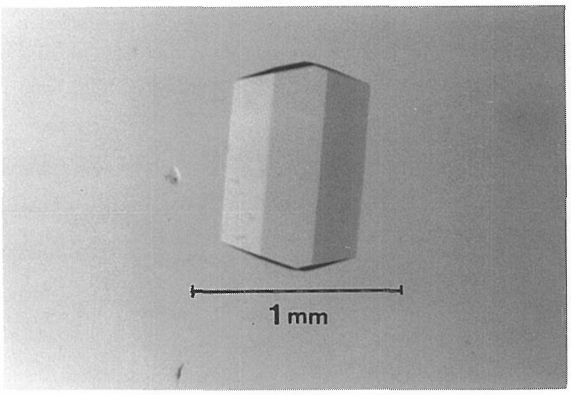

Fig. 2. A crystal of *P. aeruginosa* alkaline protease.

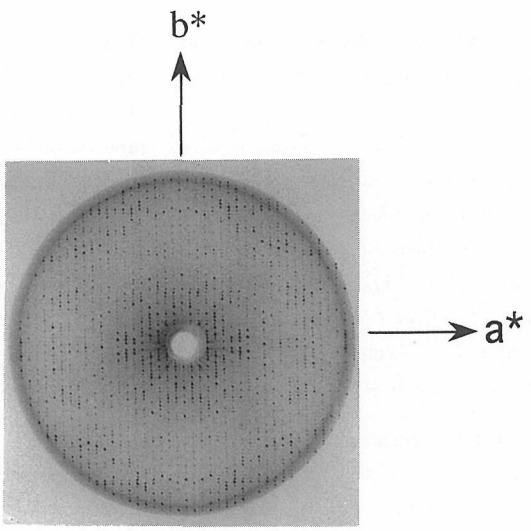

Fig. 3. An X-ray precession photograph (hk0 zone) of *P. aeruginosa* alkaline protease.

the droplet used in the previous step. The seeding was started by sealing a crystallization dish of the six droplet and four small tubes of 1 ml reservoir solution in a plastic box (105×75×28 mm). Finally, prismatic crystals (1.0×0.6×0.3 mm) suitable for X-ray experiments were obtain in one week (Fig. 2). Precession photographs showed that the crystals diffract up to at least 3 Å resolution (Fig. 3). The coarse crystal parameters obtained from precession photographs were refined for 2θ angles of 25 reflections ($5°<2\theta<25°$) measured on a Rigaku AFC-5 diffractometer using Ni-filtered CuKα radiation from a rotating anode X-ray generator (Rigaku RU-200) operated at 40 kV/100 mA. The crystals belong to space group $P2_12_12_1$ with cell dimensions a=77.16, b=176.69, c=51.12 Å. The asymmetric unit of the crystal contains one enzyme molecule, and the solvent content of the crystal is about 66% (v/v). The crystallization procedures and crystallographic parameters are summarized in Table. 1.

Table 1. Crystallization and crystallographic parameters.

Method	Vapor diffusion
Protein concentration (w/v%)	1.0
Precipitant	6% PEG 6000
pH	5.6
Temperature (°C)	25
Time (day)	7
Space group	$P2_12_12_1$
a (Å)	77.2
b (Å)	176.7
c (Å)	51.2
Z	4
V_m(Å^3)	3.56
$V_{solv.}$	0.66

2.2 Preparation of isomorphous heavy-atom derivatives

Isomorphous heavy-atom derivative crystals were prepared by soaking native crystals in heavy-atom solutions.[12] Conditions for the preparation were surveyed by recording X-ray diffraction profiles of prepared derivative crystals with a Rigaku AFC-5 diffractometer using the Ni-filtered CuKα radiation from a rotating anode X-ray generator (Rigaku RU-300) operated at 40 kV/300 mA. Three kinds of effective isomorphous derivative crystals were obtained by soaking native crystals in the heavy-atom solutions of 15 mM CH_3HgCl for 3 days, 2.5 mM $HgCl_2$ for 1 day and 1 mM $UO_2(CH_3COO)_2$ for 1 day, respectively. The derivatives showed significant intensity changes between the native crystal and each of the derivative crystals. The difference Patterson function for each derivative revealed the major site of each heavy-atom, which showed that the derivatives were all appricable to phase determination.

2.3 Data collection and processing

Diffraction intensities of the crystals were rather weak in high resolution range probably because of the high solvent content. Synchrotron radiation experiments were then required to collect intensity data of the crystals in high resolution range. All data sets for the native and three kinds of heavy-atom derivative crystals were collected with a screenless Weissenberg

camera[15] at the BL6A$_2$ station of Photon Factory in National Laboratory for High Energy Physics, Tsukuba, Japan. The monochromatic X-ray wavelength was adjusted to 1.00 Å at the station. Fuji imaging plates were used as a two-dimensional detector for recording diffraction patterns. Each of the crystals was mounted with the crystallographic c^*-axis parallel to the rotation axis of the crystal. For one Weissenberg shot, the oscillation range and the ratio of crystal rotation to cassete movement were 4.7° and 4.7°· mm^{-1}, respectively. The exposure time was 14.1 sec.. A series of diffraction images which covers a crystallographically indipendent area was recorded for the native and heavy-atom derivative crystals. Twenty five frames of the partial image for each crystal were digitized with a Fuji Film BA100 photo-reader system and processed at 2.0 Å resolution using the program WEIS.[16] Consequently, all frames of intensity data for each crystal were merged and scaled together to obtain about 32,000 independent reflections from about 67,000 reflections observed in the resolution range 50.0~2.0 Å, with Rmerge 4~6%. The conditions of the synchrotron radiation measurements are summarized in Table 2.

Table 2. Conditions of data collection.

Wavelength (Å)	1.00
Spindle axis	c^*
Overlap (deg)	0.5
Oscillation angle $\Delta\omega$ (deg)	4.7
Cassette movement ΔZ (mm)	4.7
ω/Z (deg/mm)	1.0
Collimator (mm)	0.2
Rotation speed (deg/sec)	2.0
Number of oscillations	6

2.4 Calculation of electron density map

The heavy-atom binding sites were located by difference-Patterson and difference-Fourier maps calculated with the program package PHASES.[17] The Harker peaks of each Patterson map were reasonably interpreted to locate the main site of each heavy atom. Refinement of the heavy-atom parameters was performed by an iterative method of phase determination and least-squares refinement.[13] Minor heavy-atom sites of each derivative were found by difference Fourier maps during the refinement and included in the further refinement. The refined heavy-atom parameters are listed in Table 3. The electron density map was calculated at 2.8 Å resolution by multiple isomorphous replacement method (MIR). The averaged figure of merit was 0.554 for 16,255 reflections ($|F_{obs}|>3\sigma|F_{obs}|$) in the resolution range of 10.0~2.8 Å. The resulting electron density map had some difficulties in interpretation. A solvent flattening technique[18] was effective to improve the quality of the electron density map. The twenty-eight cycles of solvent flattening were executed by gradually increasing the ratio of solvent content from 0.45 to 0.55. The averaged figure of merit was improved to 0.752. The statistics in the map calculation is shown in Table 4. The improved electron density map revealed the overall folding of the enzyme molecule. The size of the molecule was almost coincident with that of *Serratia* protease estimated by small angle X-ray scattering method[14].

Table 3. Diffraction data and statistics for calculating electron density map.

Diffraction data				
Crystals	Native	CH_3HgCl	$HgCl_2$	$UO_2(OCOCH_3)_2$
Resolution (Å)	2.0	2.0	2.0	2.0
Total observations ($I>\sigma(I)$)	69,524	66,307	66,808	67,894
Unique reflections	33,686	32,610	32,053	32,801
Completeness of data (%)	73.8	71.5	70.2	71.9
Rmerge[a] (%)	3.76	4.81	5.17	4.38

Statistics for calcutating electron density map at 2.8 Å resolutions

Derivative	Resolution (Å)	Number of sites	Phasing power[b]
CH_3HgCl	10.0~2.8	4	1.62
$HgCl_2$	10.0~2.8	6	1.53
$UO_2(OCOCH_3)_2$	10.0~2.8	6	1.56
Averaged figure of merit	0.554		

[a] Rmerge (%)$=100\Sigma_i|\langle I_i\rangle - I_i|/I_i$; $\langle I_i\rangle$ is the average of I_i over all symmery equivalents. [b] Phasing power$=\langle F_H\rangle/E$; $\langle F_H\rangle$ is the r.m.s. heavy-atom structure factor amplitude and $\langle E\rangle$ is the r.m.s. lack of closure error.

Table 4. Heavy atom parameters.

Derivative	No. of site	X	Y	Z	B	G
CH_3HgCl	1	0.5106	0.3976	0.4253	31.69	1.259
	2	0.0167	0.3993	0.1725	57.88	0.465
	3	0.0980	0.2425	0.5064	80.00	0.513
	4	0.7480	0.0837	0.3228	63.12	0.368
$HgCl_2$	1	0.0709	0.3240	0.2686	47.37	1.180
	2	0.0100	0.3996	0.1554	78.21	0.799
	3	0.0893	0.2488	0.4730	68.84	1.039
	4	0.5082	0.3973	0.4219	30.34	0.856
	5	0.7217	0.4529	0.4304	54.08	1.086
	6	0.7462	0.0829	0.3259	51.71	0.389
$UO_2(OCOCH_3)_2$	1	0.1877	0.1078	0.2686	49.87	0.684
	2	0.6800	0.2239	0.4883	45.66	1.486
	3	0.5633	0.1655	0.4448	43.60	0.387
	4	0.3305	0.0089	0.1091	55.22	0.414
	5	0.3290	0.2940	0.1562	56.78	0.311
	6	0.5076	0.4500	0.5079	67.92	0.345

B: temperature factor G: occupancy in arbitrary scale.

2.5 Model building

The solvent-flattend electron density map at 2.8 Å resolution was good enough to show the main-chain folding and most of the side-chain orientations. In spite of some ambiguities left in the map, the chain trace was not so difficult because information useful for structure determination of the present enzyme was available from structural studies of *Serratia* protease, a homologous enzyme whose structure was almost elucidated by our collaborators. The density map clearly showed the similarity in tertiary structure between both enzymes, especially around

the active site zinc atom and in the secondary structure regions. The zinc atom site could be easily assigned to the highest peak in the density map. The amino acid sequence around the zinc atom could be easily recognized on the map because many zinc-requiring metalloproteases have the conserved structure around the zinc binding site, as suggested by the consensus sequence shown in Fig. 1. An initial model of the *P. aeruginosa* alkaline protease was built by superimposing each amino acid residue on the electron density map with a computer graphic system, IRIS Indigo Elan using the program package TURBO-FRODO.[19-20] Most of the 470 residues were located in the continuous electron density humps. However, there remained some ambiguities mainly in loop regions on the surface of the molecule. To interpret these regions of the electron density map more precisely, difference-Fourier maps were calculated with coefficients of $(2|F_{obs}|-|F_{calc}|)\exp(i\alpha_{calc})$ or $(|F_{obs}|-|F_{calc}|)\exp(i\alpha_{calc})$ obtained by the omission of these ambiguos and questionable peptide segments. The active site zinc atom was positioned on the highest electron density of the $(|F_{obs}|-|F_{calc}|)\exp(i\alpha_{calc})$ map. The polypeptide region of the consensus sequence, HEXXHXXGXXH was well located around the zinc atom. Calcium sites were also assigned to electron density peaks of the $(|F_{obs}|-|F_{calc}|)\exp(i\alpha_{calc})$ map which appeared at the distances of 2.0 to 2.5 Å corresponding to those between the calcium ions and their ligand atoms of the appropriate residues. Eight peaks were assigned as calcium ions. The initial crystallographic R value between the observed and calculated structure amplitudes was 43.5% for 16,182 independent reflections within the resolution of 10.0 to 2.8 Å.

2.6 Refinement of structure

The resulting model of the structure was refined by simmulated annealing method using the molecular dynamics program X-PLOR[21-24] installed on a CRAY Y-MP2E/264 supercomputer. In preparation of simmulated annealing refinement, several cycles of energy minimization were

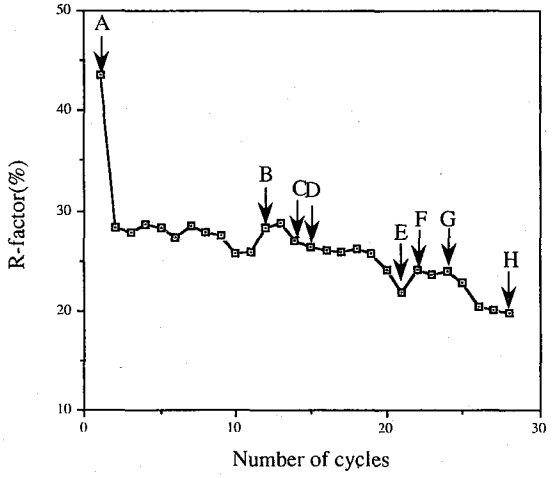

Fig. 4. Strategy and progress of structure refinement with X-PLOR : A, start of refinement with 2.8 Å initial model ; B, extension of resolution to 2.5 Å ; C, addition of 110 water oxygens and 8 calcium ions ; D, increase of the number of waters to 183 ; E, temperature factor refinement ; F, extension of resolution to 2.3 Å ; G, increase of the number of waters to 253 ; H, increase of the number of waters to 303.

carried out to relieve strains or bad contacts in the initial model. The slowcooling protocol for simulated annealing was then executed by reducing the temperature from 3,000 K to 300 K by 25. At each temperature, 50 cycles of refinement were executed. The model containing 3,501 atoms for 470 amino acid residues was initially refined for 16,182 ($|F_{obs}|>2\sigma(F_{obs})$, 92.6% comlete) reflections in the range of 10.0 to 2.8 Å. In the course of refinement, polypeptide segments which moved out of the electron density flow were modified by manual rebuilding with ($2|F_{obs}|-|F_{calc}|$) maps displayed on a computer graphics. At this stage, the crystallographic R value was converged to 0.283. After a reasonable convergence of the refinement, the resolution was gradually extended to 2.3 Å with low resolution data cut off up to 6.0 Å resolution. Water molecules were included in the further refinement at 2.5 Å resolution. The overall and restrained individual temperature factors were also refined at 2.5 Å resolution. Positional parameters and temperature factors were refined iteratively during the refinement. After several cycles of the manual rebuilding and refinement of the model structure, refinement of the structure model consisting of 470 amino acid residues, the active site zinc atom and 303 water molecules was converged to the current R value of 0.198 for 24,407 reflections ($|F_{obs}|>3\sigma(F_{obs})$, 78.7% complete) in the range of 6 to 2.3 Å resolution. The course of the refinement is shown in Fig. 4.

3. RESULTS AND DISCUSSION

The electron density map calculated with coefficients ($2|F_{obs}|-|F_{calc}|$) exp ($i\alpha_{calc}$) shows that the present model is well fitted in the electron density. The quality of the density map around the active zinc atom is demonstrated in Fig. 5. The Ramachandran plot of the model is

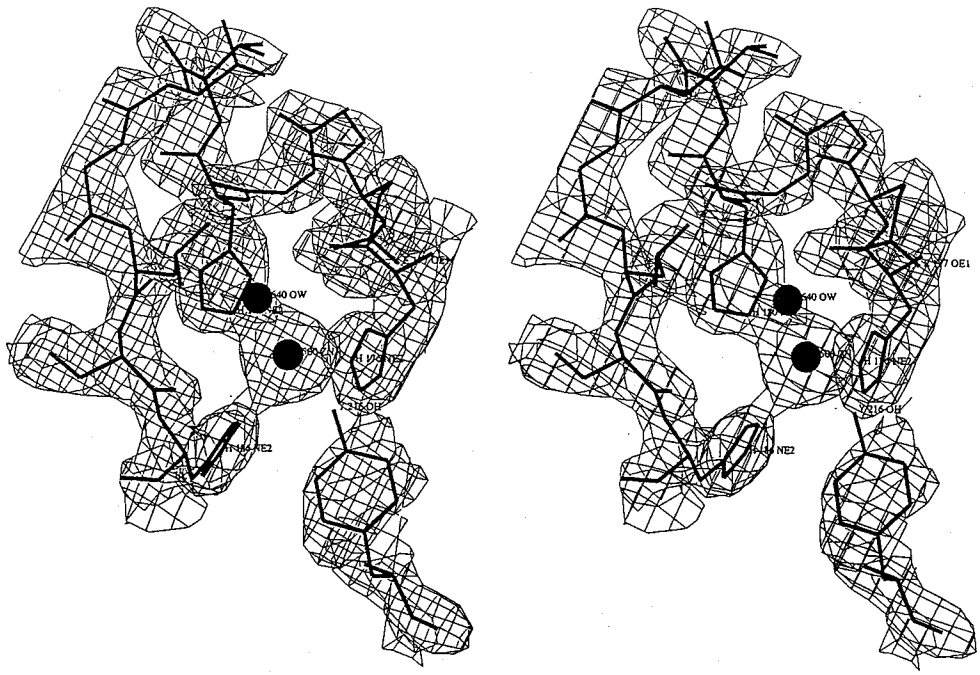

Fig. 5. A stereoview of the 2.3 Å ($2|F_{obs}|-|F_{calc}|$) map around the active site zinc ion. The contours are drawn at 1.5 σ level.

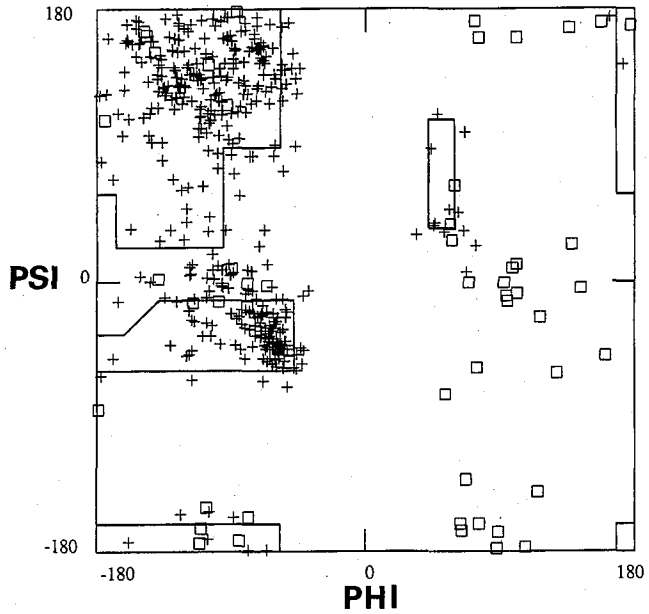

Fig. 6. Ramachandran plot of the present structure. Crosses indicate (ϕ, ψ)-conformations of non-glycine residues, and squares those of glycines.

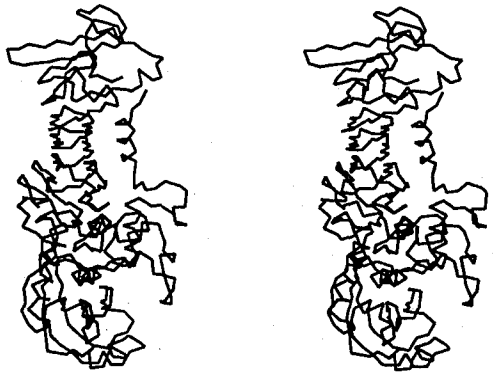

Fig. 7. A stereoview of a α-carbon trace of *P. aeruginosa* alkaline protease. The upper half is the C-terminal domain which has an unusual parrallel β-helix structure in the central region. The lower half is the N-terminal domain which is the proteolytic domain with the zinc atom inside the cleft.

shown in Fig. 6. Almost all the residues have reasonable conformations with appropriate (ϕ, ψ) values.

The stereoview of the molecular strucure of *P. aeruginosa* alkaline protease is shown in Fig. 7. The molecule has an elongated ellipsoidal shape with approximate dimensions of $90\times42\times35$ Å. The structure of the enzyme consists of two distinctive domains, as shown in Fig. 8. The N-terminal domain containing most of the N-terminal residues, 18～251, is the proteolytic domain which has a deep and wide cleft with the active site zinc atom inside. The domain consists of

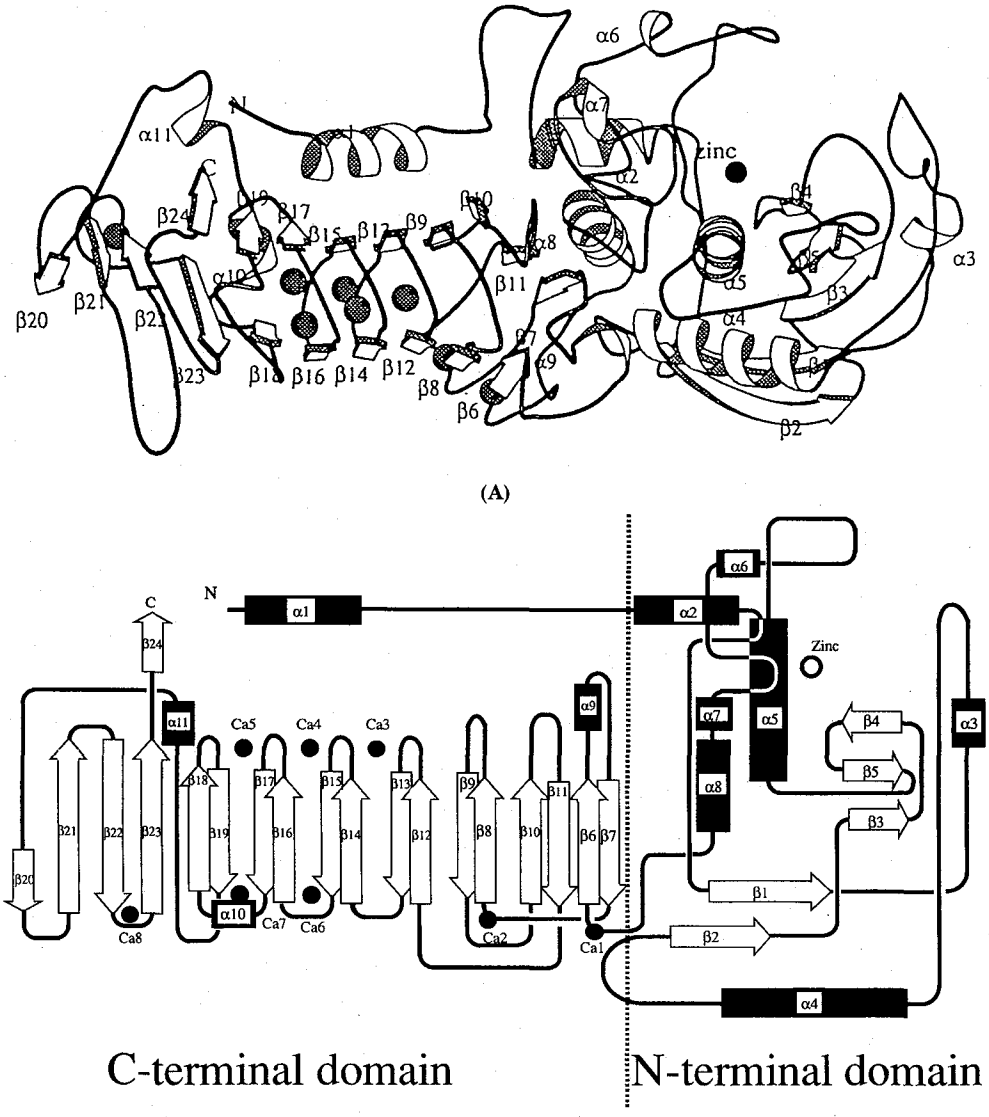

Fig. 8. (A) Ribbon drawing of *P. aeruginosa* alkaline protease. α-helices are drawn by right-handed spirals, and β-strands by arrows. The black ball is active site zinc atom, and the shaded balls are Ca^{2+} ions. This picture was drawn by a program MOLSCRIPT.[32] (B) Folding topology of the enzyme. The dotted line shows the interface between the N- and C-terminal domains. α-helices are shown by black squares, and β-strands by arrows. The white circle indicates the zinc position, and black circles indicate Ca^{2+} ion sites.

twelve elements of secondary structures : seven α helices ($\alpha 2$ to $\alpha 8$) and five β-strands ($\beta 1$ to $\beta 5$). The active site helix $\alpha 5$ lies in the vicinity of the active site zinc ion and offers two zinc ligands, H176 and H180, as well as the catalytic residue E177. Seen from the direction parallel to the helix, the shape of the cleft looks like a clear round hole whose diameter is about 15 Å. The active site zinc ion is ligated by five ligands : H176, H180 and H186 from $\alpha 5$, Y216 from the loop

between $\alpha 6$ and $\alpha 7$, and one water molecule. This system of ligation to the active site zinc ion is observed in common with other zinc-metalloproteases except thermolysin family.[25-26] The bottom of the cleft consists of helix $\alpha 4$ and a piece of a large β-sheet which consists of five β-strands, $\beta 1$ and $\beta 2$, and the remainder of the β-sheet ($\beta 1$ to $\beta 5$), $\beta 3$ to $\beta 5$, faces toward the active site helix $\alpha 5$. The loop region D189-A200 between $\alpha 5$ and $\alpha 6$ has relatively high temperature factor, as shown in Fig. 9. The region is extended over the active site cleft and might be concerned with the catalytic activity. The overall tertiary structure of the proteolytic domain is similar to that of astacin from cryfish *Astacus astacus* L., a zinc metalloprotease of another family whose structure has been determined.[27]

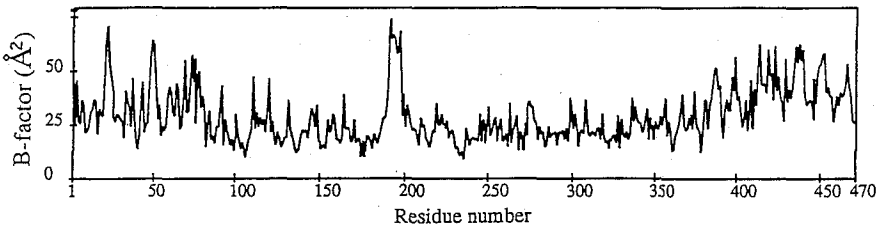

Fig. 9. A plot of average isotropic temperature-factors ($Å^2$) versus residue number.

The C-terminal domain of residues 252~470 is the β-strand-rich domain formed by nineteen β-strands, $\beta 6$ to $\beta 24$, which are incorporated in a two-layer β-sandwich structure. The domain can be subdivided into three separate regions on the basis of structural features. The amino-proximal region, which includes six strands $\beta 6$ to $\beta 11$, adopts a mixed parallel/antiparallel β-sheet topology with the irregularly wounded loops. The region is connected to the catalytic domain by the loop linking $\beta 6$ to $\alpha 8$, and is in contact with the domain through one external face of this region. The C-terminal region consisting of strands $\beta 18$ to $\beta 24$ again has a mixed β-sheet topology with rather irregular loop connection between the strands. The central region consisting of six strands $\beta 12$ to $\beta 17$ has an unusual parallel β-helix structure with all the strands regularly wound in a right-handed spiral. The N-terminal helix of the present enzyme packs predominantly on one external face of the β-sheet ($\beta 12$, $\beta 15$, $\beta 17$) of this region. In the β-helix structure, two parallel β-sheets, ($\beta 12$, $\beta 14$, $\beta 16$) and ($\beta 12$, $\beta 15$, $\beta 17$), are packed together in an antiparallel manner. The sheets of the central β-helix have only a slight twist, which is a striking contrast to parallel β-sheets found in parallel α/β domains of proteins. This flatness of the sheets in β-helix appears to be a consequence of the characteristic Ca^{2+} binding discussed below. This also stands in contrast to nature of the β-sheets in the other regions of β-sandwich structure which have more individual twists. A parallel β-helix structure similar to the central β-helix of *P. aeruginosa* alkaline protease is also found in pectate lyases C and E from *Erwinia chrysanthemi*.[28] The parallel β-helix in the pectate lyases is composed of three parallel β-sheets, two of which form a β-sandwich and the third parallel β-sheet is perpendicular to the β-sandwich. The β-helix in *P. aeruginosa* alkaline protease does not have the third parallel β-sheet that is found in pectate lyases C and E from *E. chrysanthemi*, but does have five internal Ca^{2+} ions which stabilize short turns between β-strands.

From biochemical experiments of *P. aeruginosa* alkaline protease, it has been well known that the enzyme requires a few Ca^{2+} ions per enzyme molecule to protect itself from self-catalytic

inactivation. In the later stages of refinement, difference Fourier maps revealed eight peaks that could be interpreted reasonably as the Ca^{2+} ion sites from the geometry of ligation. From the peak height in the maps, seven of the eight Ca^{2+} ion sites, Ca1-Ca7, were fully occupied and the other one Ca8 partially occupied in the β-sandwich domain. The first two Ca^{2+} ions, Ca1 and Ca2, bind in the first region of the β-sandwich domain in a 7-coordinate geometry. The next five Ca^{2+} ions, Ca3-Ca7, in the central parallel β-helix are bound internally in the short turns between the successive strands. These Ca^{2+} ions bind in a regular manner and appear to be essential for stabilization of the parallel β-helix structure. Each of the five Ca^{2+} ions is bound in an octahedral 6-coordinate geometry. Three of the Ca^{2+} ions, Ca3-Ca5, are completely buried in the internal region of the parallel β-helix and bound exclusively with the ligands from the peptide loops. The other two Ca^{2+} ions, Ca6 and Ca7, are bound in the interface between the central parallel β-helix and the C-terminal regions, and have one and two H_2O ligands, respectively.

Inspection of the sequence alignments of these Ca^{2+} binding regions as well as the parallel β-helix structure suggests that the tandemly repeated consensus sequence motif GGXGXDXBX, where X is an arbitrary residue and B is a large hydrophobic residue. The first six residues of this motif which form a short turn are involved in Ca^{2+} ion binding. X3 and X5 in the corners of the turn are preferably occupied by small hydrophobic residues. The last three residues of the sequence motif form a short β-strand. The central residue of this triplet, B, is ideally leucine, which projects nicely into the interior of the β-helix to make hydrophobic zipper-like interactions with corresponding residues on opposite β-strands. These interactions (as in a handshake) on the interface between the β-sheets appear to be essential for stabilizing the packing of β-sheets in the parallel β-helix structure. The Ca^{2+} ion binding is further essential for the parallel β-helix structure. Each GGXGXD motif provides two half-sites for Ca^{2+} binding: the first half-site consisting of main-chain carbonyls of G2 and G4, and one carboxyl oxygen of D6, and the second consisting of carbonyls of G1 and X3, and the other carboxyl oxygen of D6. Each Ca^{2+} ion is coordinated by ligands for the two different half-sites contributed by two loops, and is bound between a pair of loops in the β-helix. Consequently, the carboxyl of each D6 residue bridges a pair of Ca^{2+} ions in this coordination system. Loops on each side of the parallel β-helix structure are connected one by one through intervention of Ca^{2+} ion between the neighboring loops. This binding mode of Ca^{2+} ions is quite unique, and appears to produce structural characteristics of the parallel β-helix.

Our structural analysis reveals that alkaline protease from *P. aeruginosa* IFO3455 has two structural domains. The N-terminal domain of *P. aeruginosa* alkaline protease which includes the active site Zn^{2+} atom can be identified as the proteolytic domain. The overall tertiary folding of this domain is strikingly similar to that of astacin although the sequence identity is relatively low between both domains. This similarity in overall tertiary structure reasonably suggests that the proteolytic domains of the enzyme and astacin evolved from a common ancestor by divergent evolution. The C-terminal domain of *P. aeruginosa* alkaline protease is a two-layer β-sandwich domain including the unusual parallel β-helix structure built of a succession of the GGXGXDXBX motif which is also detected in the case of hemolysin.[29-31] This domain does not appear to be directly involved in the enzymatic activity. Since the repeats of the consensus sequence motif can form the stable β-helix structure by binding Ca^{2+} ions in the interior of the helix, it seems reasonable to suggest that the absence of Ca^{2+} ions should result in the instability

of this structure. Such instability could easily make the polypeptide unfolded and facilitate membrane translocation of the polypeptide in an unfolded form. After secretion of alkaline protease from *P. aeruginosa*, the polypeptide could be folded into a well-defined structure by the unique binding of Ca^{2+} ions present in the extracellular medium. Thus, it may be suggested that the Ca^{2+} binding region of *P. aeruginosa* alkaline protease may have some role in the folding of the molecule after transmembrane translocation in secretion processes. *P. aeruginosa* alkaline protease and related bacterial proteases which are secreted from Gram-negative bacteria are well known to share some features : presence of inactive zymogen, utilization of similar export systems which do not require an N-terminal signal sequence, and presence of multiple repeats of the consensus sequence motif for Ca^{2+} binding. These common features suggest that the enzymes may have similar β-helix structures which are related to a common functon. Some possible roles for the parallel β-helix structure have been suggested so far, but their possibilities should be checked carefully by further experiments.

ACKNOWLEDGMENTS

We are deeply indebted to Drs. Noriyoshi Sakabe and Atsushi Nakagawa, Photon Factory, National Laboratory of High Energy Physics, for their kind support in synchrotron experiments. We would like to express our sincere thanks Dr. Kensaku Hamada, Departement of Science, Shimane University, for his informative discussion on structural similarity between *P. aeruginosa* alkaline protease and *Serratia* protease.

The computation in this work was performed partly in the Supercomputer Laboratory, Institute for Chemical Research, Kyoto University, and the Research Center for Protein Engineering, Institute for Protein Research, Osaka University. We would like to thank all the staffs in the computation centers for their kind help in our computation.

REFERENCES

(1) K. Okuda, K. Morihara, Y. Atsumi, H. Takeuchi, S. Kawamoto, H. Kawasaki, K. Suzuki and J. Fukushima, *Infect. Immun.*, **58**, 4083 (1990).
(2) F. Duong, A. Lazdunski, B. Cami and M. Murgier, *Gene*, **121**, 47 (1992).
(3) K. Morihara, *Biochim. Biophys. Acta*, **73**, 113 (1963).
(4) K. Morihara and H. Tsuzuki, *Biochim. Biophys. Acta*, **92**, 3510 (1964).
(5) K. Morihara, T. Hiroshige and O. Tatsushi, *Biochim. Biophys. Acta*, **309**, 414 (1973).
(6) K. Morihara, *Kagaku to Seibutu*, **14**, 798 (1991).
(7) Y. Shibuya, T. Yamamoto, T. Morimoto, N. Nishino, T. Kambara and H. Okabe, *Biochim. Biophys. Acta*, **1077**, 316 (1991).
(8) K. Morihara and K. Okuda, *Seikagaku*, **64**, 1499 (1992).
(9) W. Stocher and D. Auld, *Biochem.*, **29**, 10418 (1990).
(10) B. Vallee and D. Auld, *Biochem.*, **29**, 5647 (1990).
(11) Y. Katsuya, K. Hamada, Y. Hata, N. Tanaka, M. Sato, Y. Katsube, K. Kakiuchi and K. Miyata, J. *Biochem.*, **98**, 11392 (1985).
(12) A. McPherson, "Preparation and Analysis of Protein Crystals", John Wiley & Sons Inc. New York, N.Y., pp. 181 (1982).
(13) R.E. Dicherson, F.C. Kendrew and B.E. Strandberg, *Acta Crystallogr.*, **14**, 1188 (1961).
(14) Y. Katsuya, Doctoral Thesis, Osaka University (1989).
(15) N. Sakabe, *J. Appl. Crystallogr.*, **16**, 542 (1983).
(16) T. Higashi, *J. Appl. Crystallogr.*, **22**, 9 (1989).
(17) W. Furey and S. Swaminathan, *Am. Crystallogr. Assoc. Mtg. Abst. Ser.*, **218**, 73 (1989).

(18) B.C. Wang, *Methods Enzymol.*, **115**, 90 (1985).
(19) T.A. Jones, *J. Appl. Crystallogr.*, **11**, 268 (1978).
(20) "TURBO-FRODO Manual, Version 5.02", Bio-Graphics Inc., (1994).
(21) A.T. Brunger, *J. Mol. Biol.*, **203**, 803 (1983).
(22) A.T. Brunger, *Acta Crystallogr.*, **A46**, 585 (1990).
(23) A.T. Brunger, *Science*, **235**, 458 (1987).
(24) A.T. Brunger, "X-PLOR Mannual, Version 3.1", Yale University Press, New Haven, U.S.A. (1992).
(25) W. Bode, F. Gomis-Ruth, R. Huber, R. Zwilling and W. Stocher, *Nature*, **358**, 164 (1992).
(26) D. Hangauer, F. Arthur and B. Matthews, *Biochem.*, **23**, 5730 (1984).
(27) B. Matthews, J. Jansonius, P. Colman, B. Sbhoenborn and D. Dupourge, *Nature New Biol.*, **238**, 37 (1972).
(28) M.D. Yonder, S.E. Lietzke and F. Jurnak, *Structure*, **1**, 241 (1993).
(29) T. Felmlee, S. Pellett and R. Welch, *J. Bacteriol.*, **163**, 94 (1985).
(30) A. Koronakis, M. Cross, B. SEnior, E. Koronakis and C. Hughes, *J. Bacteriol.*, **169**, 1509 (1987).
(31) N. Mackman, J. Nicaud L. Gray and I. Holland, *Mol. Gen. Genet.*, **201**, 529 (1985).
(32) P. Kraulis, *Appl. Crystallogr.*, **24**, 946 (1991).